Enhanced annealing stability and perpendicular magnetic anisotropy in perpendicular magnetic tunnel junctions using W layer

Jyotirmoy Chatterjee, Ricardo C. Sousa, Nicolas Perrissin, Stéphane Auffret, Clarisse Ducruet, Bernard Diény

Enhanced annealing stability and perpendicular magnetic anisotropy in perpendicular magnetic tunnel junctions using W layer

Jyotirmoy Chatterjee, Ricardo C. Sousa, Nicolas Perrissin, Stéphane Auffret, Clarisse Ducruet, and Bernard Dieny

Citation: Appl. Phys. Lett. **110**, 202401 (2017); doi: 10.1063/1.4983159
View online: https://doi.org/10.1063/1.4983159
View Table of Contents: http://aip.scitation.org/toc/apl/110/20
Published by the American Institute of Physics

Enhanced annealing stability and perpendicular magnetic anisotropy in perpendicular magnetic tunnel junctions using W layer

Jyotirmoy Chatterjee,[1] Ricardo C. Sousa,[1] Nicolas Perrissin,[1] Stéphane Auffret,[1] Clarisse Ducruet,[2] and Bernard Dieny[1]
[1]*University Grenoble Alpes/CEA-INAC/CNRS, SPINTEC, 38000 Grenoble, France*
[2]*Crocus Technology, 4 place Robert Schuman, 38000 Grenoble, France*

(Received 28 February 2017; accepted 21 April 2017; published online 15 May 2017)

The magnetic properties of the perpendicular storage electrode (buffer/MgO/FeCoB/Cap) were studied as a function of annealing temperature by replacing Ta with W and W/Ta cap layers with variable thicknesses. W in the cap boosts up the annealing stability and increases the effective perpendicular anisotropy by 30% compared to the Ta cap. Correspondingly, an increase in the FeCoB critical thickness characterizing the transition from perpendicular to in-plane anisotropy was observed. Thicker W layer in the W(t)/Ta 1 nm cap layer makes the storage electrode highly robust against annealing up to 570 °C. The stiffening of the overall stack resulting from the W insertion due to its very high melting temperature seems to be the key mechanism behind the extremely high thermal robustness. The Gilbert damping constant of FeCoB with the W/Ta cap was found to be lower when compared with the Ta cap and stable with annealing. The evolution of the magnetic properties of bottom pinned perpendicular magnetic tunnel junctions (p-MTJ) stack with the W2/Ta1 nm cap layer shows back-end-of-line compatibility with increasing tunnel magnetoresistance up to the annealing temperature of 425 °C. The pMTJ thermal budget is limited by the synthetic antiferromagnetic hard layer which is stable up to 425 °C annealing temperature while the storage layer is stable up to 455 °C. *Published by AIP Publishing.*
[http://dx.doi.org/10.1063/1.4983159]

Spin transfer torque magnetic random access memories (STT-MRAM) are the focus of intense research and development efforts due to their non-volatility, low-energy consumption, high-speed performance, quasi-infinite endurance, and reliability.[1–3] Especially, perpendicular magnetic tunnel junctions (pMTJs) used for STT-MRAM applications offer better downsize scalability and trade-off between retention and write power consumption than their in-plane magnetized counterparts.[2–5] The core of pMTJ is the *FeCoB (reference)/MgO/FeCoB (storage layer)/cap layer* stack. To achieve high tunnel magnetoresistance (TMR) and high perpendicular magnetic anisotropy (PMA), a post-deposition annealing is carried out. This anneal yields an improvement in the crystallinity of the MgO barrier, a crystallization of the FeCoB by gettering B out of the magnetic layers,[6,7] and a sharpening of the bcc (100) MgO/FeCo interface.[8] In general, the higher the annealing temperature, the better the crystallinity.[5–7] However, it was observed that above a certain annealing temperature, the TMR and PMA deteriorates[9] due to diffusion of non-magnetic species toward the tunnel barrier, especially of Ta when this material is inserted next to the FeCoB layer. This diffusion mechanism limits the thermal budget that a pMTJ stack can tolerate.[10,11] Using the Ta cap layer, it is difficult to obtain pMTJs with a high PMA storage layer (SL) and back-end-of-line (BEOL) annealing tolerance which is 400 °C for 30 min. Hence, a detailed investigation of magnetic properties of the top storage layer as a function of annealing temperature was carried out using the W material in the cap layer. Previous works reported on improvement in PMA of FeCoB with W and Mo buffer or cap layers associated with increasing annealing temperature up to 450 °C.[12,13] However, thicker MgO barriers were used in these studies, yielding a very high resistance-area (RA) product (∼100 kΩ μm^2). Here, we report a record high stability upon annealing up to 570 °C without compromising RA values (∼15 Ω μm^2) by using a composite W/Ta cap layer. Moreover, we also bring deeper insights into the physical-chemical origin of this enhanced annealing stability.

We performed a systematic study of the dependence on annealing temperature of the magnetic properties of the pMTJ top electrode storage layer [*Ta 3/MgO∼1/FeCoB 1.2 nm/Cap*] using Ta, W, and W/Ta cap layers of different thicknesses. W in the cap layer improves the PMA by 30% and annealing stability compared with the Ta cap layer. Using the MgO cap, though the PMA can be almost doubled, it also increases the RA value.[14,15] Moreover, it cannot provide as high thermal budget as W/Ta. Increasing the W thickness in W(t)/Ta 1 nm cap layer enhances the annealing stability of the stack. A record annealing stability of the storage layer (570 °C for 30 min) was demonstrated using the W5/Ta1 nm cap layer. This is attributed to the overall stiffening of the stack due to the large mechanical hardness of W (melting temperature of 3422 °C). Similar improvements in the resistance to interdiffusion upon high temperature anneals were observed earlier in spin-valves when a thin nano-oxide layer was introduced in the stack to form so-called specular spin-valves.[16,17] Other benefits of the W insertion come from the much reduced W interdiffusion, thanks to strong W-W chemical bonds and reduced B diffusion towards the barrier layer, which were observed by chemical characterization by secondary ion mass spectroscopy (SIMS). In addition, the magnetic and transport properties of the Co/Pt

multilayers synthetic antiferromagnet (SAF) based bottom pinned perpendicular magnetic tunnel junctions (p-MTJ) stack with the W2/Ta1 nm cap were studied as a function of annealing temperature. This stack exhibits thermal robustness with increasing TMR up to 425 °C. The dependence of the Gilbert damping constant, α, on the annealing temperature was also characterized in the FeCoB 2.5 nm layer by ferromagnetic resonance (FMR) spectroscopy. α is more stable upon annealing and has lower values for the W2/Ta1 nm cap than for Ta 5 nm cap.

The samples were deposited on the Si wafer by magnetron sputtering under an Ar pressure of 2×10^{-3} mbar. The MgO tunnel barrier was obtained by naturally oxidizing a 0.8 nm thick metallic Mg layer under an oxygen pressure of 3×10^{-2} mbar with a flow rate of 100 sccm for 240 s. On top of this oxidized layer, a second Mg layer 0.5 nm thick was deposited. The resistance-area (RA) product for these oxidation conditions is 15 Ω μm^2. All the samples were annealed for 30 min at different temperatures under a high vacuum (5×10^{-6} mbar). The anisotropy energy is calculated from the area between perpendicular and in-plane M(H) loops measured using a vibrating sample magnetometer (VSM). The magnetic properties, such as amplitude of the Kerr signal, coercivity, remanence of stacks deposited on 100 mm Si wafers with crossed wedges of $Fe_{72}Co_8B_{20}$ and Mg, were mapped by the magneto optical Kerr effect (MOKE) measurement. Using this technique, we could find out the optimum FeCoB and Mg thicknesses for which the anisotropy is maximum, the critical thickness of FeCoB above which the magnetization becomes in-plane and the magnetic dead layer thickness. Figure 1(a) illustrates the layer configuration of the top storage electrode with Ta, W, and W/Ta cap layers. The bottom 4Å FeCoB layer is magnetically dead and is only used to promote better growth of MgO. The storage layer with the Ta cap layer was used as a reference stack for comparison of PMA and thermal budget of other stacks. Figure 1(b) shows the effective perpendicular magnetic anisotropy energy density (K_{eff}) of the storage electrode as a function of annealing temperature for different types of cap layers. The value of effective perpendicular anisotropy energy density (K_{eff}) for the Ta 1 nm cap layer is 1.6×10^6 erg/cm^3 after annealing at 340 °C. By increasing the Ta cap layer thickness to 2 nm, K_{eff} remains stable up to 400 °C anneal likely due to an improved B gettering efficiency of the thicker Ta cap. This value is increased by 30% (2.1×10^6 erg/cm^3) when the W layer is used in the cap layer. Moreover, the thermal budget that the stack can tolerate also increases. Figure 2 shows the out-of-plane M(H) loops for the stacks with the W(t)/Ta 1 nm cap layers, where W thickness was varied from 1 to 5 nm in 1 nm steps. The magnetic reversal of the samples remains sharp with high squareness before the PMA reduction starts occurring at 485 °C for W1/Ta. The temperature characterizing the beginning of the K_{eff} degradation increases with W thickness and reaches more than 570 °C for W5/Ta1 nm. Above the degradation temperature, the M(H) loops exhibit hard axis magnetic characteristics with the perpendicular applied field. The thermal budget without the 1 nm Ta layer on top of W is comparatively lower. Figure 3 shows K_{eff} vs. annealing temperature for these storage electrodes showing that the thicker W layer makes the stack more robust against annealing. However, varying W thickness does not change the PMA of the storage layer. The sample with the W5/Ta1 nm cap shows stable PMA with sharp and square M(H) loop without any reduction of coercivity even after annealing at 570 °C. This is the highest annealing tolerance temperature ever reported for perpendicular half-MTJs.[12,13] To get a deeper understanding on this enhanced thermal robustness with thicker W, secondary ion mass spectrometry (SIMS) depth profiling was carried out for the stacks with the W2/Ta1 and W5/Ta1 cap. The results are presented in Figure 4. For the sake of clarity, we selectively chose few elements to show in the SIMS profiles and a separate graph for B profile. W being a very stiff metal with a very high melting point (3422 °C), W-W covalent bonds are very robust, preventing W diffusion to take place in the investigated range of annealing temperatures as observed in the SIMS profile. Upon annealing, B diffuses towards W which acts as a boron absorber. However, for W2/Ta1, a significant B diffusion towards MgO is also observed after annealing at 570 °C (see Fig. 4(a)), which degrades the FeCoB/MgO interfacial magnetic properties by yielding a significant PMA loss as shown in Fig. 3. With W5, B diffusion towards MgO is not observed. Therefore, thicker W is believed to improve the stack s annealing stability by stiffening the overall structure and efficiently absorbing the B away from the MgO interface with possibly W-borides formation.

Since the PMA is improved using W in the cap layer, it is worth to find out whether the critical FeCoB thickness up to which PMA is maintained is larger than that for the Ta cap. In order to calculate the critical thicknesses as a function of annealing temperature, two samples with the layer

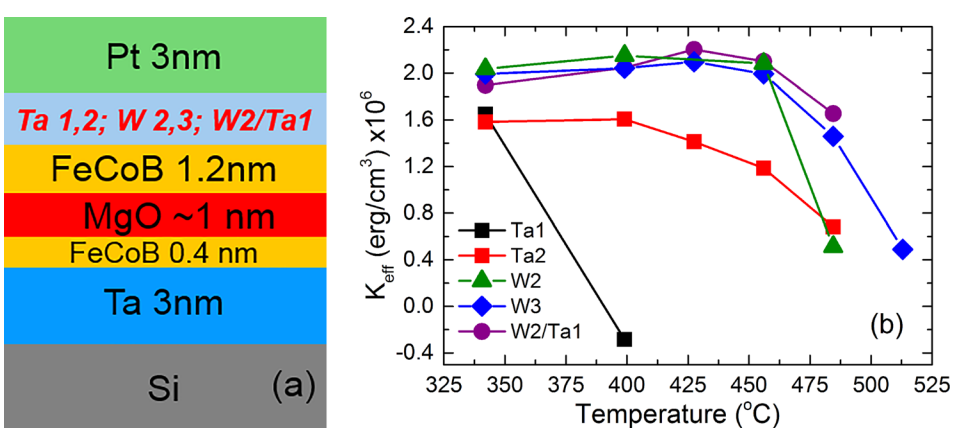

FIG. 1. (a) Schematic drawing of top electrode half-MTJ stack and (b) effective perpendicular anisotropy (K_{eff}) as a function of annealing temperature.

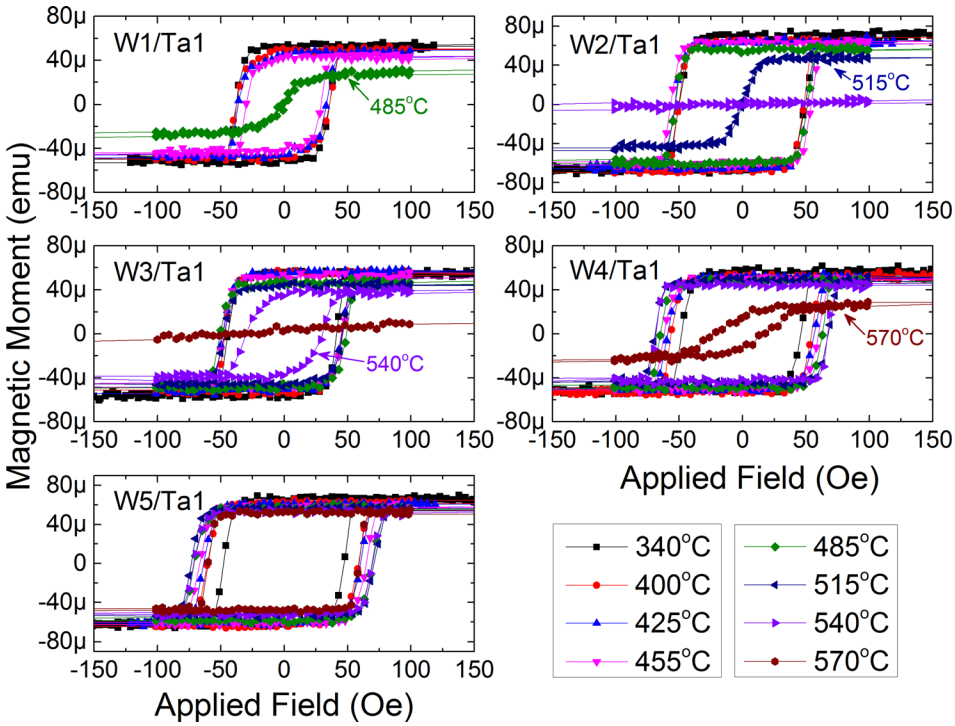

FIG. 2. Out-of-plane M(H) loops of half-MTJs with W (1, 2, 3, 4, and 5)/Ta 1 nm cap as a function of annealing temperature.

configuration *Ta3/MgO/FeCoB (wedge)/cap (Ta 1) or (W 2/Ta 1)/Pt 2 nm* were deposited. The MOKE amplitude of FeCoB was plotted as function of thickness to extract the critical thickness (t_c) as well as magnetic dead layer thickness (t_d). Figure 5 shows one of these plots for the stack with the W2/Ta1 cap after annealing at 425 °C. At a low thickness (<1.1 nm), though the FeCoB is perpendicular, due to poor crystallinity and defects, FeCoB magnetization is low and its hysteresis loop does not show 100% remanence. Above that thickness, the hysteresis loop of FeCoB becomes square with 100% remanence. From this thickness, the MOKE amplitude increases linearly due to the linear increase of total magnetization. The magnetic dead layer thickness of the FeCoB layer was calculated from a linear fit of the amplitude in this region by extrapolation to the thickness where the total magnetization becomes zero (see the blue dotted line in Fig. 5). After the 100% remanence zone, when the FeCoB thickness further increases, the magnetization gradually rotates from perpendicular to in-plane. The critical thickness above which the FeCoB becomes in-plane was extracted by linear extrapolation of the MOKE amplitude vs. thickness plot in the transition region and intersection with the zero amplitude. The values of t_c together with the values of t_d at different annealing temperatures are listed in Table I, showing

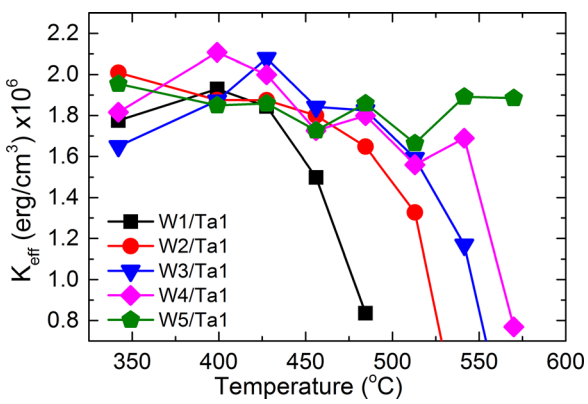

FIG. 3. K_{eff} of half-MTJs with W (1, 2, 3, 4, and 5)/Ta 1 nm cap as a function of annealing temperature.

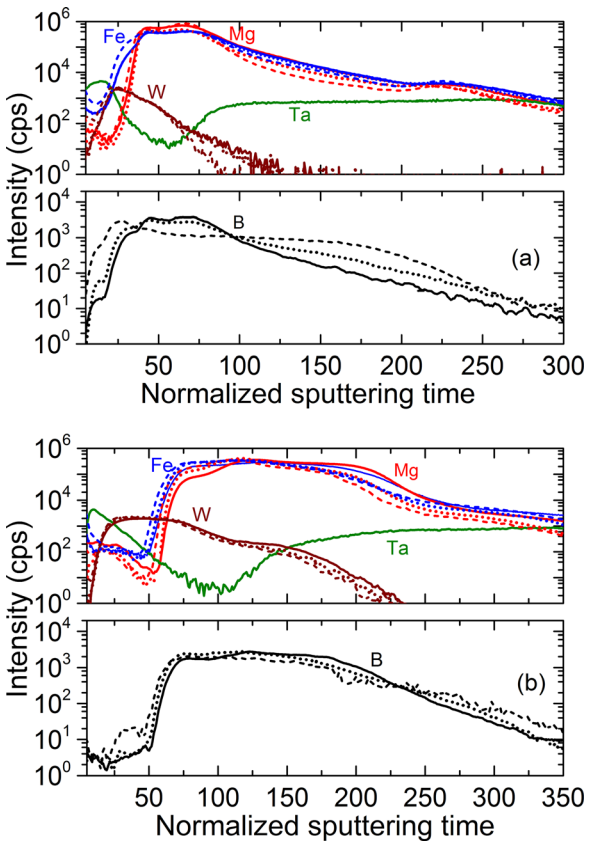

FIG. 4. The SIMS depth profile of half-MTJ stacks with (a) W2/Ta1 and (b) W5/Ta1 nm cap layers. Solid line represents the as deposited sample, dotted line represents the 340 °C annealed sample, and dashed line represents the 570 °C annealed sample.

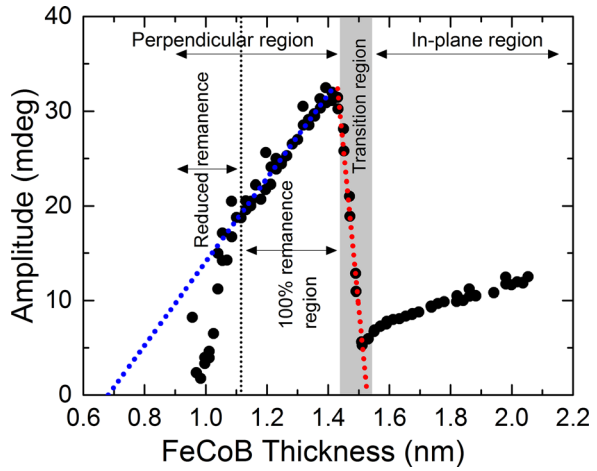

FIG. 5. Amplitude of the Kerr Signal as a function of FeCoB thickness with the W2/Ta1 nm cap after annealing at 425 °C.

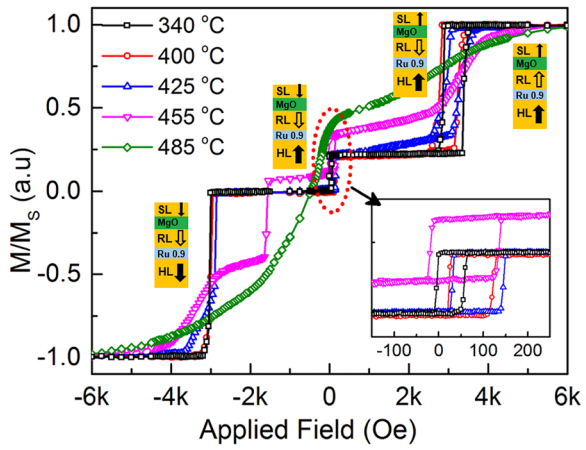

FIG. 6. Normalized out-of-plane M(H) loops of pMTJ stack at different annealing temperatures measured by VSM. The inset shows minor loops of the storage (free) layer.

higher values of critical thickness associated with the W/Ta cap. The values of t_d are observed to be similar at 340 °C. Therefore, the value of the effective critical magnetic thickness (t_c-t_d) up to which out-of-plane anisotropy is preserved is larger for W/Ta than for the Ta cap.

After having focused on the magnetic properties of the top electrode storage layer and investigated the role of W in the cap layer, we studied the magnetic and transport properties of full pMTJ stacks as a function of annealing temperature by VSM and the current in-plane tunneling (CIPT) method. The layer configuration of pMTJ stack was *Si/bottom electrode/Pt 5/(Co/Pt) ML based SAF/Ta 0.3/FeCoB 1.2/Mg 0.7/Oxidation-30s/Mg 0.5/FeCoB 1.4/W 2/Ta 1/Pt 3 nm*. The resistance-area (RA) product for this oxidation condition is 8 Ω μm^2. The SAF layer consists of a hard layer (HL: *[Co 0.5/Pt 0.25]$_6$/Co 0.5 nm*) and a reference layer (RL: *[Co 0.5/Pt 0.25]$_3$/Co 0.5/Ta 0.3/FeCoB 1.2 nm*) antiferromagnetically coupled to a 0.9 nm Ru layer. Figure 6 shows out-of-plane M(H) loops of the pMTJ films after annealing at various temperatures. The magnetic reversal of all the magnetic layers, *e.g.*, SL, RL, and HL are indicated by the arrows when the magnetic field is swept from +6 kOe to −6 kOe. The reversal steps are very sharp and well separated from each other after annealing at 400 °C. At 425 °C, the switching of the RL and HL become slightly canted but still well separated from each other. The coercivity of RL reduces to 180 Oe at 425 °C from 230 Oe and 260 Oe at 400 °C and 340 °C, respectively, which is calculated from the minor loop of RL.

TABLE I. Critical thickness (t_c) and dead layer thickness (t_d) after annealing at different annealing temperatures (T_A).

	Ta 1 nm cap		W2/Ta1 nm cap	
T_A (°C)	t_c (Å)	t_d (Å)	t_c (Å)	t_d (Å)
315	14.3	4.6	…	…
340	13.6	6	15.5	6.05
400	…	…	15.3	6.75
425	…	…	15.3	6.8
455	…	…	15.1	7

After annealing at 455 °C, the PMA of the RL degrades drastically, and the coercivity becomes zero. Moreover, the HL also shows a canted reversal along with vertical reversal steps. However, the free layer is still perpendicular with high squareness and a coercivity of 76 Oe, as shown in the inset of Fig. 6. The dependence on annealing temperature of the TMR of the pMTJ stacks and of patterned devices are shown in Fig. 7. For CIPT measurement on blanket pMTJ films, a CuN bottom electrode was used. The graph shows that TMR increases with annealing temperature and reaches 104% at 400 °C. Above 400 °C, the PMA of the SAF layer degrades significantly for the CuN electrode, resulting in a reduced TMR. In contrast, the patterned devices with a 80 nm diameter exhibit a higher TMR ratio of 117% after annealing at 425 °C. This is because the SAF layer of the pMTJ stack was deposited on the Ta/Ru/W/Ta electrode, making it magnetically more stable than when grown on the CuN electrode required for CIPT measurements. Annealing at high temperature improves the crystalline quality of the MgO barrier and that of the SL,[8] yielding a higher TMR up to 425 °C. The Gilbert damping constant of 2.5 nm FeCoB with Ta and W/Ta caps annealed at different temperatures were measured by ferromagnetic resonance (FMR) in an in-plane geometry. Approximately 4×1 mm^2 samples were placed upside-down on a RF coplanar waveguide mounted on a 0.96 T electromagnet.

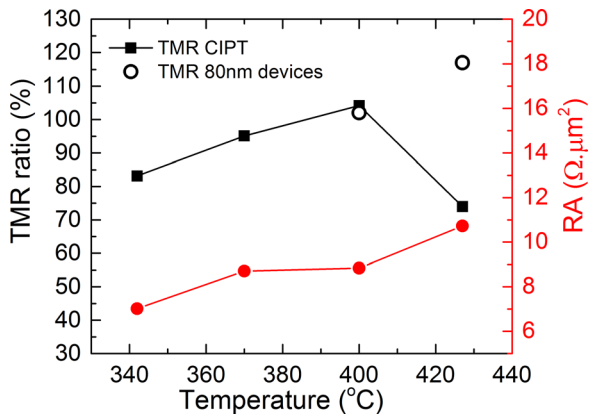

FIG. 7. TMR as a function of temperature measured by the CIPT method and on 80 nm diameter patterned devices.

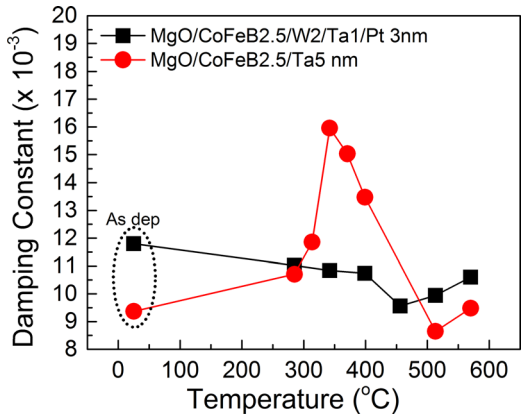

FIG. 8. The Gilbert damping constant of FeCoB as a function of annealing temperature for Ta and W/Ta cap layers extracted by ferromagnetic resonance spectroscopy.

Measurements were carried out for RF frequencies ν from 2 to 24 GHz. The in-plane Kittel equation describes the resonance condition, $\nu = \frac{\gamma\mu_0}{2\pi}\sqrt{H_{res}(H_{res}+M_s^{eff})}$, where M_s^{eff} is the effective magnetization and $\gamma = \mu_B g_{eff}/\hbar$, the gyromagnetic ratio with μ_B the Bohr magneton, $\hbar$ the reduced Plank's constant, and g_{eff} the effective g-factor. The Gilbert damping constant α is extracted using the frequency dependence of the resonance linewidth, $\Delta H = \Delta H_0 + \frac{2}{\sqrt{3}}\frac{\alpha}{\gamma}2\pi\nu$. The intercept ΔH_0 is smaller than 5 Oe for all samples, indicating negligible contribution from inhomogeneous broadening. The FeCoB damping constant with the Ta cap layer increases with temperature, reaching a maximum at 350 °C as shown in Fig. 8. Above this temperature, α decreases again to the initial value. In contrast, α remains constant in the whole temperature range for the W/Ta cap layer. Although the annealing temperature dependent variation of α with the Ta cap is not clear at this moment, we speculate that this evolution could be associated with Ta interdiffusion, which is inhibited in the case of the W/Ta cap layer. Therefore, α remains constant for W/Ta cap layers. Moreover, α is lower for W/Ta cap layers in the temperature range of 350–400 °C, which is the range used for both stand-alone and embedded application.

In conclusion, we have demonstrated a 30% PMA enhancement and significant improvement in annealing stability of the storage layer using W in the cap layer compared with the Ta cap layer. Thicker W in the W(t)/Ta 1 nm cap layer further improves the annealing stability of the stack, thanks to a stiffening effect of the W layer and its ability to efficiently absorb the B away from the MgO interface. Record annealing stability of storage electrode up to 570 °C was demonstrated using a W 5/Ta 1 nm cap. Clear magnetic reversal of pMTJ stacks with the W2/Ta1 nm cap with the increasing TMR ratio up to 117% were achieved after annealing at 425 °C, which is more than the thermal budget for BEOL process. Moreover, the Gilbert damping constant of FeCoB with the W cap has been found to be lower and more stable as a function of annealing temperature than with the Ta cap.

This work was supported by the French National Research Agency by the EXCALYB project, by the European Union under the ERC MAGICAL project (No. 669204) and by LabEx Minos ANR-10-LABX-55–01.

[1]S. Mangin, D. Ravelosona, J. A. Katine, and E. E. Fullerton, Nat. Mater. **5**, 210 (2006).
[2]S. Ikeda, K. Miura, H. Yamamoto, K. Mizunuma, H. D. Gan, M. Endo, S. Kanai, J. Hayakawa, F. Matsukura, and H. Ohno, Nat. Mater. **9**, 721 (2010).
[3]J. Sun, Phys. Rev. B **62**, 570 (2000).
[4]L. Thomas, G. Jan, J. Zhu, H. Liu, Y. J. Lee, S. Le, R. Y. Tong, K. Pi, Y. J. Wang, D. Shen, R. He, J. Haq, J. Teng, V. Lam, K. Huang, T. Zhong, T. Torng, and P. K. Wang, J. Appl. Phys. **115**, 172615 (2014).
[5]T. Kishi, H. Yoda, T. Kai, T. Nagase, E. Kitagawa, M. Yoshikawa, K. Nishiyama, T. Daibou, M. Nagamine, M. Amano, S. Takahashi, M. Nakayama, N. Shimomura, H. Aikawa, S. Ikegawa, S. Yuasa, K. Yakushiji, H. Kubota, a. Fukushima, M. Oogane, T. Miyazaki, and K. Ando, in 2008 IEEE International Electron Devices Meeting (2008), p. 1.
[6]S. Yuasa, Y. Suzuki, T. Katayama, and K. Ando, Appl. Phys. Lett. **87**, 242503 (2005).
[7]X. Kozina, S. Ouardi, B. Balke, G. Stryganyuk, G. H. Fecher, C. Felser, S. Ikeda, H. Ohno, and E. Ikenaga, Appl. Phys. Lett. **96**, 072105 (2010).
[8]S. V. Karthik, Y. K. Takahashi, T. Ohkubo, K. Hono, S. Ikeda, and H. Ohno, J. Appl. Phys. **106**, 023920 (2009).
[9]J. Chatterjee, T. Tahmasebi, J. Swerts, G. S. Kar, and J. De Boeck, Appl. Phys. Express **8**, 063002 (2015).
[10]M. Yamanouchi, R. Koizumi, S. Ikeda, H. Sato, K. Mizunuma, K. Miura, H. D. Gan, F. Matsukura, and H. Ohno, J. Appl. Phys. **109**, 07C712 (2011).
[11]S. Ikeda, J. Hayakawa, Y. Ashizawa, Y. M. Lee, K. Miura, H. Hasegawa, M. Tsunoda, F. Matsukura, and H. Ohno, Appl. Phys. Lett. **93**, 082508 (2008).
[12]G. G. An, J. Bin Lee, S. M. Yang, J. H. Kim, W. S. Chung, and J. P. Hong, Acta Mater. **87**, 259 (2015).
[13]W. Skowroński, T. Nozaki, D. D. Lam, Y. Shiota, K. Yakushiji, H. Kubota, A. Fukushima, S. Yuasa, and Y. Suzuki, Phys. Rev. B: Condens. Matter Mater. Phys. **91**, 184410 (2015).
[14]B. Rodmacq, S. Auffret, B. Dieny, and L. E. Nistor, U.S. patent application 8,513,944 B2 (2013).
[15]H. Sato, T. Yamamoto, M. Yamanouchi, S. Ikeda, S. Fukami, K. Kinoshita, F. Matsukura, N. Kasai, and H. Ohno, Tech. Dig. - Int. Electron Devices Meet. **2013**, 3.2.1.
[16]S. H. Jang, T. Kang, H. J. Kim, and K. Y. Kim, Appl. Phys. Lett. **81**, 105 (2002).
[17]S. Y. Yoon, Y. I. Kim, D. H. Lee, Y. S. Kim, D. H. Yoon, and S. J. Suh, Mater. Sci. Eng. B: Solid-State Mater. Adv. Technol. **110**, 265 (2004).